Gradient-index phononic crystal lens-based enhancement of elastic wave energy harvesting

S. Tol, F. L. Degertekin, and A. Erturk

View Online　　　**Export Citation**　　　**CrossMark**

ARTICLES YOU MAY BE INTERESTED IN

Gradient-index phononic crystal lens-based enhancement of elastic wave energy harvesting

S. Tol, F. L. Degertekin, and A. Erturk[a)]

G. W. Woodruff School of Mechanical Engineering, Georgia Institute of Technology, Atlanta, Georgia 30332, USA

We explore the enhancement of structure-borne elastic wave energy harvesting, both numerically and experimentally, by exploiting a Gradient-Index Phononic Crystal Lens (GRIN-PCL) structure. The proposed GRIN-PCL is formed by an array of blind holes with different diameters on an aluminum plate, where the blind hole distribution is tailored to obtain a hyperbolic secant gradient profile of refractive index guided by finite-element simulations of the lowest asymmetric mode Lamb wave band diagrams. Under plane wave excitation from a line source, experimentally measured wave field validates the numerical simulation of wave focusing within the GRIN-PCL domain. A piezoelectric energy harvester disk located at the first focus of the GRIN-PCL yields an order of magnitude larger power output as compared to the baseline case of energy harvesting without the GRIN-PCL on the uniform plate counterpart. *Published by AIP Publishing.*
[http://dx.doi.org/10.1063/1.4960792]

Over the last decade, various methods of energy harvesting have been researched toward enabling next-generation self-powered electronic devices for wireless applications ranging from structural health monitoring to wearable electronic components.[1–4] Many research groups worked on scavenging ambient energy such as waste heat, solar, vibration, and flow energy in order to power small electronic components. Among the alternative transduction techniques for harvesting structural vibrations and kinetic energy, piezoelectric transduction has become the most popular method due to the ease of application and high power density of piezoelectric materials.[5–7] While the harvesting of standing waves and vibrations has been well investigated, the potential of traveling wave energy in fluids and structures, i.e., propagating acoustic and elastic waves, has received much less attention. Relatively few research efforts have explored this area with a focus on polarization-patterned piezoelectric solids,[8] quarter-wavelength resonators,[9] hydraulic pressure fluctuations,[10] Helmholtz resonators,[11–13] phononic crystals,[14–17] or one-dimensional bending wave energy harvesters.[18] Wave propagation approach to energy harvesting enables the possibility of extracting the maximum electrical power in propagating wave scenarios including transient excitations and offers an insight that is otherwise not easily available in standing wave or modal vibration methods. Importantly, to improve the efficiency of electrical power generation, it is required to develop proper strategies for elastic wave energy localization and focusing. To this end, recently, elliptical and parabolic mirrors composed of acoustic scatterers have been implemented in order to focus propagating flexural waves (A_0 mode Lamb wave) for enhanced piezoelectric energy harvesting.[19,20] The harvested energy can also be enhanced by designing acoustic metamaterials which focus or properly localize the wave energy by tailoring wave propagation characteristics. For instance, Gradient-Index Phononic Crystal Lens (GRIN-PCL) proposed by Lin *et al*.[21] was designed with solid cylinders embedded in an epoxy medium such that the refractive index along the direction transverse to the phononic wave propagation had a hyperbolic secant gradient distribution. Hence, the incident waves were bent gradually toward the center axis where the refractive index was the highest (or the wave speed was the lowest), resulting in convergence at a focal spot. Later, focusing of the A_0 mode Lamb wave in a perforated silicon GRIN-PCL plate was demonstrated numerically by Wu *et al*.[22] and further explored both numerically and experimentally by Zhao *et al*.[23] In both studies, GRIN-PCL was designed for high frequency Lamb waves on the order of 7–10 MHz.

In this work, we present a detailed experimental and numerical investigation of a blind hole-based GRIN-PCL structure and couple it with piezoelectric transduction for dramatically enhanced elastic wave energy harvesting. First, we show the focusing of the low frequency A_0 Lamb wave mode in an aluminum plate by implementing a GRIN-PCL with a blind hole-based unit cell design. The hyperbolic secant gradient distribution is obtained by tailoring the unit cell diameter of the blind holes. Then, we employ the resulting GRIN-PCL for the performance enhancement in structure-borne elastic energy harvesting from the A_0 mode Lamb waves originating from a line source. Our goal is to implement a metamaterial design that can focus the incident plate wave energy at a focal spot where the piezoelectric energy harvester is located to maximize the electrical power output. In the existing literature, GRIN-PCLs have been demonstrated (mostly numerically) by means of material,[21] diameter,[21] and height[25] variations of the periodically arranged stubs, or hole size variation of the perforated plates,[23,26] or local variations of plate thickness.[24,27] In the present work, we extend the elastic wave GRIN-PCL concept to a blind hole crystal structure setting (rather than

a)Author to whom correspondence should be addressed. Electronic mail: alper.erturk@me.gatech.edu

perforated) which is critical for practical implementations, and then we implement the design in the context of energy harvesting from elastic waves. The GRIN-PCL based on the blind hole unit cell structure of different diameters used in this work can be more advantageous as compared to complete perforation and external stubs in practical applications since mass addition (of bulky stubs) is avoided while structural integrity (unlike though hole scenarios) is better preserved.

The blind hole distribution is based on the hyperbolic secant gradient profile, which was calculated from dispersion curves. We used finite element analysis (COMSOL Multiphysics) to calculate band structures of A_0 mode propagating along the ΓX orientation in PCs for various filling factors (ff $= \pi d^2/4a^2$) with an aluminum plate thickness of $h = 3.175$ mm, blind hole depth of $h_b = 2.175$ mm, and unit cell size of $a = 8$ mm (as illustrated by Fig. 1(a)). Figure 1(b) shows that the frequency band of the A_0 mode drops and the group velocity decreases with increased ff at the design frequency (50 kHz). Note that this frequency is chosen merely to demonstrate and validate the concept using a GRIN-PCL setup with compact dimensions and is not intended for a specific application. As is common practice in energy harvesting, the design frequency (and therefore the resulting GRIN-PCL dimensions) would be dictated by the given excitation spectrum.

The refractive index profile of a two dimensional, continuous GRIN medium along the transverse direction (y-axis) can be defined as[21]

$$n(y) = n_0 \operatorname{sech}(\alpha y), \quad (1)$$

where n_0 is the refractive index along the center axis and α is the gradient coefficient. For small anisotropy as displayed in Fig. 1(c) and waves propagating predominantly along x-direction, the refractive index of the A_0 mode can be approximated by the refractive index along the ΓX direction as

$$n = \frac{\upsilon}{\upsilon_{\Gamma X}} = \frac{\upsilon}{d\omega/dk_{\Gamma X}}, \quad (2)$$

where $\upsilon_{\Gamma X}$ is the group velocity along the ΓX direction and υ is the reference group velocity of the A_0 mode in a homogenous aluminum plate of the same thickness (evaluated at 50 kHz). Based on the concept described by Wu et al.,[22] we optimized the GRIN-PCL design to obtain the refractive index profile shown in Fig. 2(a). The refractive index values were calculated as $n = [1.186, 1.178, 1.155, 1.117, 1.068, 1.010]$ for filling factor values of ff $= [0.601, 0.589, 0.539, 0.440, 0.284, 0.049]$ corresponding to 2.175 mm blind hole depth with diameter $d = [7.000, 6.930, 6.630, 5.990, 4.810, 2.000]$ mm, at $y = [0, \pm1a, \pm2a, \pm3a, \pm4a, \pm5a]$, respectively. The gradient coefficient was determined as $\alpha = 0.1164$, resulting in the first focal point at $13.5a$ (i.e., $\pi/2\alpha$) and second focal point at $40.5a$, both of which can be observed from the analytically obtained beam trajectory[28] shown in Fig. 2(b).

Figure 3 shows the fabricated GRIN-PCL plate including 51 blind holes along the propagation direction of the A_0 mode Lamb waves originating from a line source. This particular GRIN-PCL plate size (especially the length) was
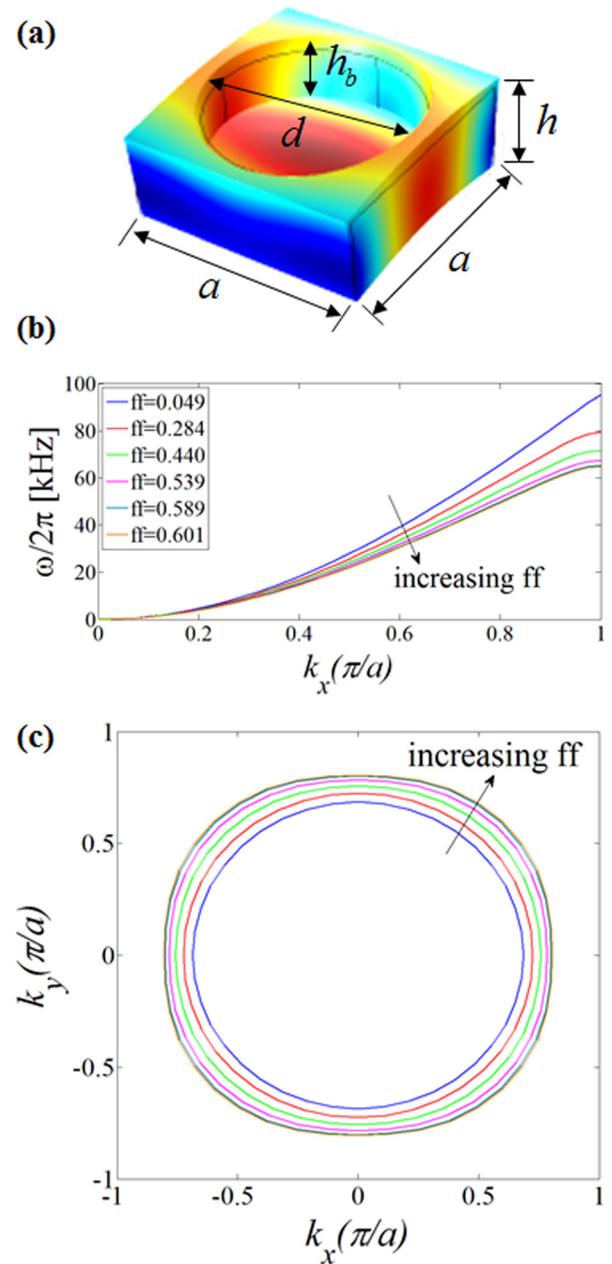

FIG. 1. (a) Schematic of the square unit cell structure of the GRIN-PCL plate with blind holes. (b) Band structure of the A_0 mode for various filling factors (ff $= \pi d^2/4a^2$). (c) Equal frequency contours of the A_0 mode Lamb wave at 50 kHz.

chosen to show focusing and defocusing of flexural waves at two focal points. Plane wave-like wave front was generated by an array of 7 mm × 7 mm × 0.2 mm piezoelectric transducers (from STEMiNC Corp.) bonded to the aluminum plate with 8 mm spacing. These transducers were excited by 4 cycles of sinusoidal burst at desired frequencies using a function generator (Agilent 33220A) and a voltage amplifier (Trek Model PZD350). Polytec PSV-400 scanning laser vibrometer was used to measure the resulting wave field by recording the out-of-plane component of the velocity of the plate over a grid of points covering the GRIN-PCL domain. With proper triggering of the laser measurements, the wave field was reconstructed. The RMS (root-mean-square) values were obtained by integrating the measured response over time.
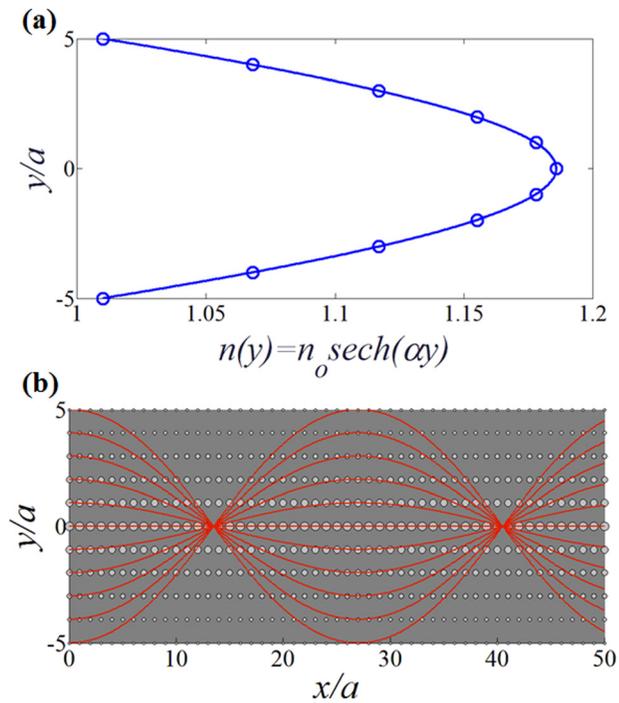
FIG. 2. (a) Hyperbolic secant profile (curve fit) and the effective refractive indices for each row (circles) at 50 kHz. (b) Beam trajectory in the proposed GRIN-PCL design hosted by an aluminum plate.
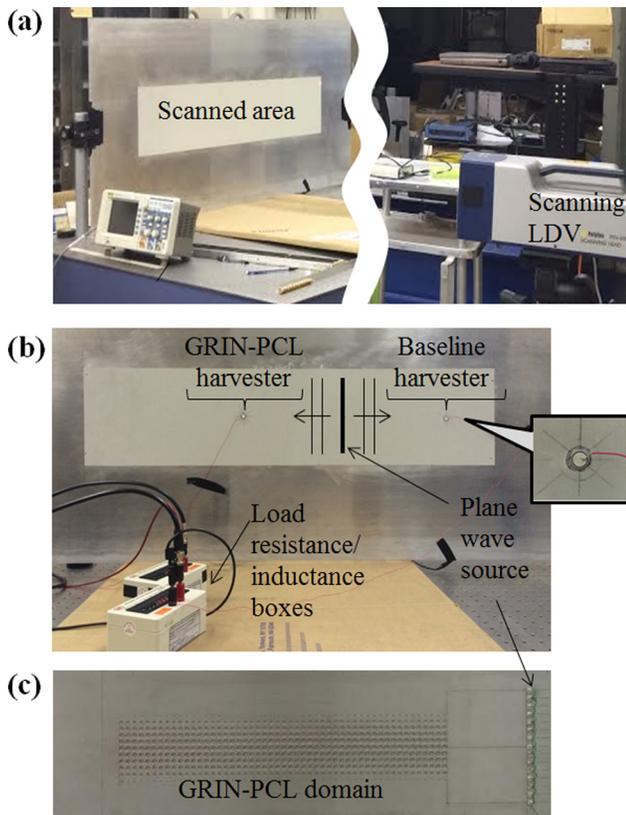

FIG. 3. Experimental setup: (a) Scanning LDV is employed for out-of-plate velocity field measurement. (b) Wave propagation domain showing the plane wave source along with the two harvesters, one at the GRIN-PCL focus and the other at the same distance from the source in the flat plate domain (as a baseline) – a close-up view of one of the identical harvester disks and resistance/inductance boxes are also shown. (c) Close-up view of the fabricated GRIN-PCL domain on the other face of the aluminum plate is displayed along with the plane wave source (made from a piezoelectric line array actuated in phase).

Figure 4(a) shows the measured RMS velocity field for excitation at various frequencies (in 30–70 kHz range) around the target (design) frequency of 50 kHz and reveals excellent agreement with the beam trajectory predictions at the target frequency (cf. Fig. 2(b)). The wave energy is focused with the maximum intensity at $x = 13.7a$ and $x = 41.2a$ along the propagation direction in the GRIN-PCL domain, which is in good agreement with the first two analytical focal points evaluated at $x = 13.5a$ and $x = 40.5a$, respectively. The maximum wave amplitude at the focus was measured to be 3.7 times of the amplitude near the source. Although the GRIN-PCL was designed to work at 50 kHz, frequency dependence of its focusing characteristics is also captured in Fig. 4(a). It is observed that the focusing neck becomes longer and the first focal points shift away from the source as the excitation frequency decreases. This can be
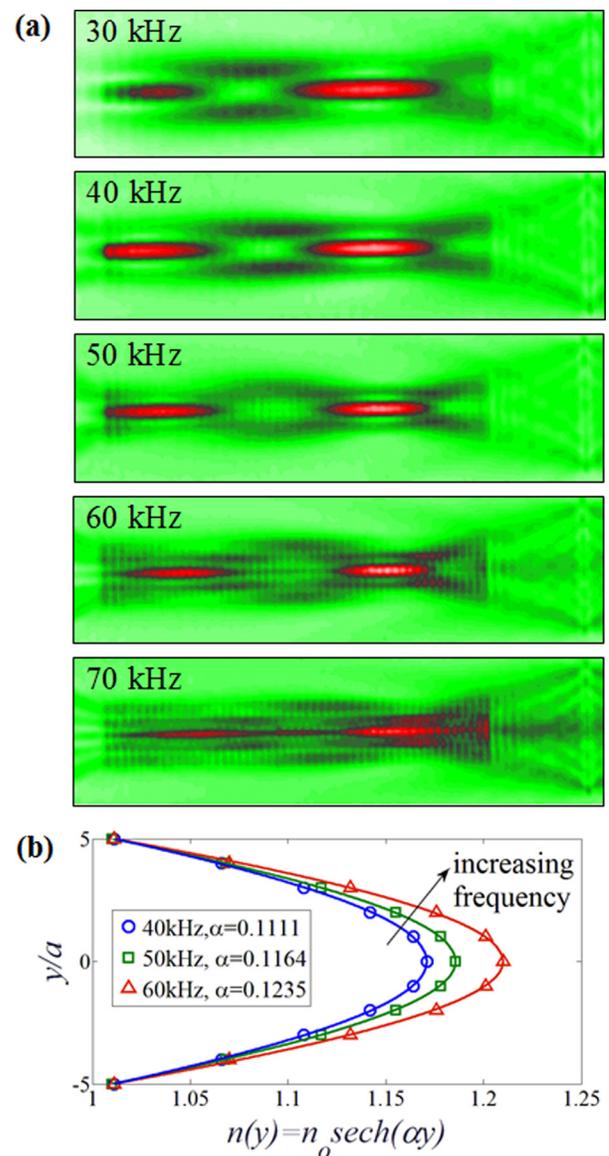

FIG. 4. (a) Experimental RMS wave field for excitations at various frequencies: 30 kHz, 40 kHz, 50 kHz, 60 kHz, and 70 kHz. The first two focal points are clearly visible at $x \sim 13.5a$ and $x \sim 40.5a$ in good agreement with the beam trajectory predictions at 50 kHz. (b) Hyperbolic secant profile curves for different excitation frequencies. Note that the gradient coefficient (α) increases/decreases with increased/decreased frequency (relative to the design frequency), yielding shorter/longer focal distance.

explained by the redistribution of the refractive index of the PC layers due to the sensitivity of the gradient coefficient to frequency.[26] As illustrated in Fig. 4(b), the gradient coefficient decreases for frequencies lower than the designed one, resulting in a larger focal distance. Similarly, the gradient coefficient α increases with increased frequency, resulting in a smaller focal distance. On the other hand, above 60 kHz, the group velocity almost vanishes for the greatest filling factor corresponding to the central unit cells of the GRIN-PCL and the wave field may be distorted due to the dominance of the evanescent waves. Note that the size of the focus region in the incident wave direction in Fig. 4(a) is dictated by the width of the GRIN-PCL (in the sense of a relative aperture).

Instantaneous wave fields under 50 kHz burst sine excitation captured at different time instances are shown in Fig. 5. This figure further demonstrates the functionality of the GRIN-PCL and provides information on the GRIN-PCL performance[23,29] and harvester optimization. For example, measurements of the reflected wave fronts show that the reflections from the GRIN-PCL are very small ($\sim$7% of the incident power), so that the incident field is focused to the harvester without significant reflection from the GRIN-PCL domain. The instantaneous wave field in the focal region shown in Fig. 5(b) is also useful in order to select the harvester dimensions, e.g., half-wavelength harvester is a reasonable choice.

Having validated the fabricated GRIN-PCL design and its focusing performance experimentally, energy harvesting performance enhancement associated with the GRIN concept is discussed next. The harvester dimensions were determined according to the wave propagation characteristics in the focal region discussed previously. As shown in Fig. 3(b), identical piezoelectric energy harvester disks were bonded at the first

focal point in GRIN-PCL domain and also in a baseline setting at the same distance from the excitation source in the uniform plate region. The two 0.4-mm-thick piezoelectric disks (STEMINC Corp.) with the half-wavelength diameter (for the design frequency of 50 kHz) are attached to the aluminum plate by means of a vacuum bonding technique that was described elsewhere.[30] Energy harvesting experiments were performed with resistor sweep tests by shunting the bottom and top electrodes of the piezoelectric harvesters to a range of resistive electrical loads covering the optimal conditions of both the GRIN-PCL-enhanced harvester and the baseline harvester. The average power output of the harvesters was calculated from the voltage measurements across the resistor with an oscilloscope (Tektronix TDS2024). Voltage response waveforms under the 2200 Ω optimal load resistance ($\sim 1/(\omega C_p)$, where C_p is the piezoelectric capacitance) are displayed in Fig. 6(a). Average power harvester from the wave

FIG. 6. Samples of voltage response histories of the GRIN-PCL harvester and the baseline harvester at 50 kHz (a) under optimal resistive loading (2200 Ω) and (b) under optimal resistive-inductive loading (20 kΩ, 6 mH). (c) RMS voltage and average power output performance curves in response to a 4-cycle 50 kHz sine burst excitation for a set of resistive loads revealing more than an order of magnitude increase in the harvested power with the GRIN-PCL structure.
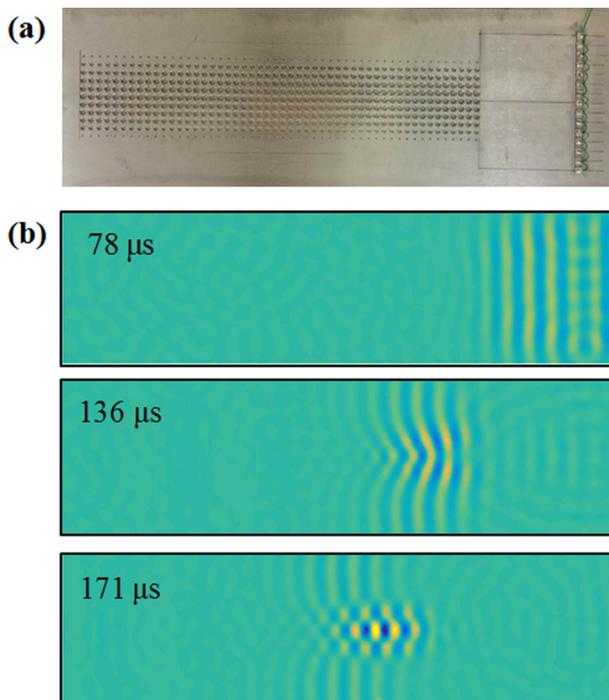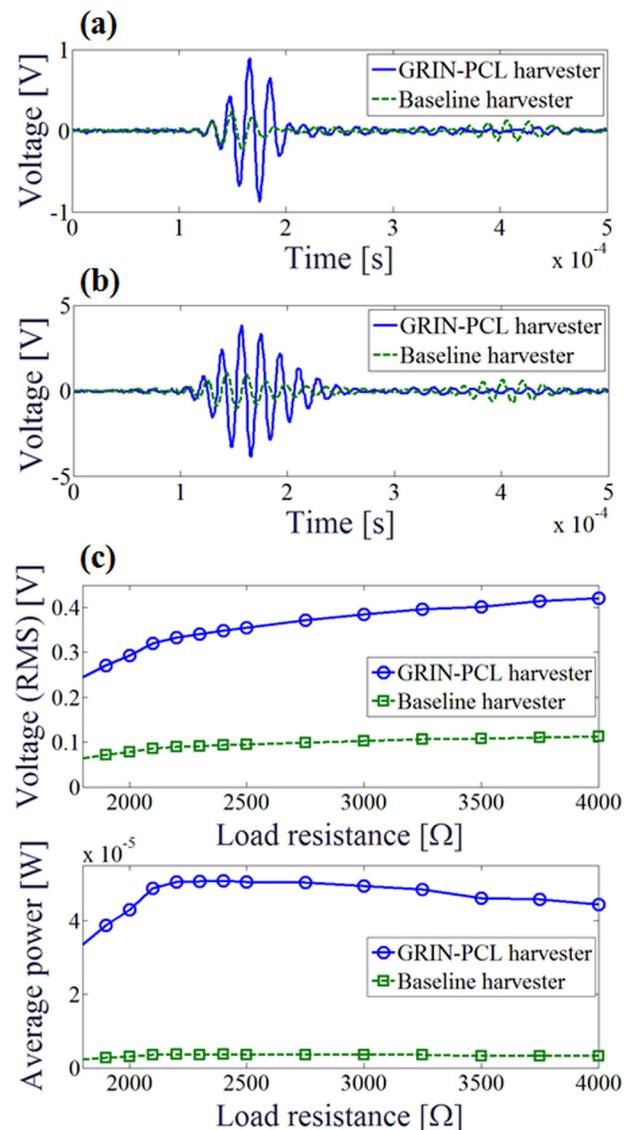

FIG. 5. (a) GRIN-PCL domain in the experimental setup and (b) out-of-plane wave field under 50 kHz burst excitation at three different time instances confirming the focusing behavior.

packet was calculated from the RMS of the voltage wave-forms and illustrated for the case of resistive loading in Fig. 6(c). Under the same excitation applied to both harvesters, the efficiency is increased by 13.8 times by focusing the elastic waves in the GRIN-PCL as compared to the baseline case of harvesting incident plane waves using an identical piezoelectric disk without the lens. Hence, the GRIN-PCL concept integrated with piezoelectric energy harvester results in dramatically enhanced structure-borne wave energy harvesting performance by more than an order of magnitude. Furthermore, the electrical power output can be boosted by improving the electrical circuit with complex load impedance matching.[18] Accordingly, under the resistive inductive loading with the optimal resistive and inductive load combination of 20 kΩ and 6 mH, the harvester voltage is increased by 5 times compared to purely resistive loading (Fig. 6(b)). The harvested power can be further enhanced by employing patterned electrodes[20] that match the field distribution shown in Fig. 5(b).

In summary, we designed, fabricated, and experimentally validated a GRIN-PCL-enhanced elastic wave energy harvester that is composed of blind holes as unit cells with varying diameters combined with a piezoelectric energy harvester disk located at its first focal point. The blind hole-based design of the GRIN-PCL (with unit cells of different diameters to have a hyperbolic secant profile of the refractive index) eliminates mass addition (unlike GRIN-PCLs with stub attachments) and offers better structural integrity (as compared to perforated GRIN-PCLs with through holes) while enhancing the harvested power output (and therefore the efficiency) by more than an order of magnitude as compared to a baseline harvester in the uniform plate domain.

[1]S. Roundy, P. K. Wright, and J. M. Rabaey, *Energy Scavenging for Wireless Sensor Networks with Special Focus on Vibrations* (Springer, New York, 2004).
[2]S. Priya and D. J. Inman, *Energy Harvesting Technologies* (Springer, New York, 2009).
[3]A. Erturk and D. J. Inman, *Piezoelectric Energy Harvesting* (Wiley, 2011).
[4]N. Elvin and A. Erturk, *Advances in Energy Harvesting Methods* (Springer, 2013).
[5]S. R. Anton and H. A. Sodano, Smart Mater. Struct. **16**(3), R1 (2007).
[6]A. Cook-Chennault, N. Thambi, and A. M. Sastry, Smart Mater. Struct. **17**, 043001 (2008).
[7]A. Erturk, Comput. Struct. **106**, 214–227 (2012).
[8]C. J. Rupp, M. L. Dunn, and K. Maute, Appl. Phys. Lett. **96**, 111902 (2010).
[9]B. Li, A. J. Laviage, J. H. You, and Y. Kim, Appl. Acoust. **74**, 1271–1278 (2013).
[10]K. A. Cunefare, E. Skow, A. Erturk, J. Savor, N. Verma, and M. Cacan, Smart Mater. Struct. **22**(2), 025036 (2013).
[11]S. B. Horowitz, M. Sheplak, L. N. Cattafesta III, and T. Nishida, J. Micromech. Microeng. **16**, S174 (2006).
[12]F. Liu, A. Phipps, S. Horowitz, K. Ngo, L. Cattafesta, T. Nishida, and M. Sheplak, J. Acoust. Soc. Am. **123**, 1983–1990 (2008).
[13]A. Yang, P. Li, Y. Wen, C. Lu, X. Peng, J. Zhang, and W. He, Appl. Phys. Expr. **6**, 127101 (2013).
[14]Z. S. Chen, Y. M. Yang, Z. M. Lu, and Y. T. Luo, Phys. B: Condens. Matter **410**, 5–12 (2013).
[15]S. Gonella, A. C. To, and W. K. Liu, J. Mech. Phys. Solids **57**(3), 621–633 (2009).
[16]W. C. Wang, L. Y. Wu, L. W. Chen, and C. M. Liu, Smart Mater. Struct. **19**, 045016 (2010).
[17]L. Y. Wu, L. W. Chen, and C. M. Liu, Appl. Phys. Lett. **95**, 013506 (2009).
[18]S. Tol, F. L. Degertekin, and A. Erturk, Wave Motion **60**, 20–34 (2016).
[19]M. Carrara, M. Cacan, J. Toussaint, M. Leamy, M. Ruzzene, and A. Erturk, Smart Mater. Struct. **22**(6), 065004 (2013).
[20]M. Carrara, J. Kulpe, S. Leadenham, M. J. Leamy, and A. Erturk, Appl. Phys. Lett. **106**, 013907 (2015).
[21]S. C. S. Lin, T. J. Huang, J. H. Sun, and T. T. Wu, Phys. Rev. B **79**, 094302 (2009).
[22]T. T. Wu, Y. T. Chen, J. H. Sun, S. C. S. Lin, and T. J. Huang, Appl. Phys. Lett. **98**, 171911 (2011).
[23]J. Zhao, R. Marchal, B. Bonello, and O. Boyko, Appl. Phys. Lett. **101**(26), 261905 (2012).
[24]Y. Jin, D. Torrent, Y. Pennec, Y. Pan, and B. Djafari-Rouhani, J. Appl. Phys. **117**, 244904 (2015).
[25]X. Yan, R. Zhu, G. Huang, and F. G. Yuan, Appl. Phys. Lett. **103**, 121901 (2013).
[26]T. T. Wu, M. J. Chiou, Y. C. Lin, and T. Ono, Proc. SPIE **8994**, 89940G (2014).
[27]A. Climente, D. Torrent, and J. Sanchez-Dehesa, Appl. Phys. Lett. **105**, 064101 (2014).
[28]C. Gómez-Reino, M. V. Perez, and C. Bao, *Gradient-Index Optics: Fundamentals and Applications* (Springer, Berlin, 2002).
[29]H. Kurt and D. S. Citrin, Opt. Express **15**(3), 1240–1253 (2007).
[30]S. R. Anton, A. Erturk, and D. J. Inman, Smart Mater. Struct. **19**(11), 115021 (2010).